Three Dimensional Photonic Dirac Points in Metamaterials

Qinghua Guo,[1,2] Biao Yang,[2] Lingbo Xia,[2,3] Wenlong Gao,[2] Hongchao Liu,[2]
Jing Chen,[4] Yuanjiang Xiang,[1,*] and Shuang Zhang[2,†]
[1]Key Laboratory of Optoelectronic Devices and Systems of Ministry of Education and Guangdong Province, College of Optoelectronic Engineering, Shenzhen University, Shenzhen 518060, China
[2]School of Physics and Astronomy, University of Birmingham, Birmingham B15 2TT, United Kingdom
[3]Center for Terahertz Waves and College of Precision Instrument and Optoelectronics Engineering, Tianjin University, Tianjin 300072, China
[4]MOE Key Laboratory of Weak-Light Nonlinear Photonics, School of Physics, Nankai University, Tianjin 300071, China
(Received 23 June 2017; published 20 November 2017)

Topological semimetals, representing a new topological phase that lacks a full band gap in bulk states and exhibiting nontrivial topological orders, recently have been extended to photonic systems, predominantly in photonic crystals and to a lesser extent metamaterials. Photonic crystal realizations of Dirac degeneracies are protected by various space symmetries, where Bloch modes span the spin and orbital subspaces. Here, we theoretically show that Dirac points can also be realized in effective media through the intrinsic degrees of freedom in electromagnetism under electromagnetic duality. A pair of spin-polarized Fermi-arc-like surface states is observed at the interface between air and the Dirac metamaterials. Furthermore, eigenreflection fields show the decoupling process from a Dirac point to two Weyl points. We also find the topological correlation between a Dirac point and vortex or vector beams in classical photonics. The experimental feasibility of our scheme is demonstrated by designing a realistic metamaterial structure. The theoretical proposal of the photonic Dirac point lays the foundation for unveiling the connection between intrinsic physics and global topology in electromagnetism.

DOI: 10.1103/PhysRevLett.119.213901

Topological phases [1–4], first arising from the quantum Hall effect [5], have fundamentally revolutionized our understanding of the states of matter. In recent years, the novel concepts of topological phases have been transferred to photonic systems, leading to the discoveries of a photonic analogy of the quantum Hall effect [6,7], 2D and 3D photonic topological insulators [8–12], and Weyl and Dirac degeneracies [13–23]. These have remarkably enriched classical photonics, opening a path towards studying fundamental new states of light and possible revolutionary applications in edge or surface optics.

Dirac point is a fourfold band crossing defined in three dimensional momentum space, away from which the energy band exhibits a linear dispersion along an arbitrary direction. As a central gapless topological phase, Dirac semimetal bridges conventional insulators, topological insulators, and Weyl semimetals. By breaking either time reversal (T) or inversion symmetry (P), it may split into two Weyl points of opposite chirality. In photonics, fourfold degeneracy of the Dirac point is usually achieved through various space symmetries in photonic crystals, where the Bloch modes, i.e., spatial degrees of freedom, play vital roles [11,12,21].

In this Letter, by utilizing the intrinsic polarization degrees of freedom, we theoretically demonstrate a way to design photonic Dirac points in a medium with homogeneous effective electromagnetic properties, merely protected by electromagnetic duality symmetry, which is usually enabled by a fixed ratio between all the permittivity and permeability tensor elements [9,12]. At the interface between air and the Dirac metamaterials, there exist spin-dependent topological surface states, which are the electromagnetic counterparts of Fermi arcs in an electronic system. Because of the linearity of their k-space dispersion, the surface waves propagate nearly without diffraction, which is significant for information transport and imaging applications. Because of the underlying topological relations, the topological charges discovered in classical photonics, such as vector or vortex beams, can be generated through the interaction of light with photonic Dirac points.

Here we first consider a uniaxial metamaterial with realistic resonant features in both permittivity and permeability. Specifically, the effective parameters of Dirac metamaterials are taking the form of $\overleftrightarrow{\varepsilon} = \mathrm{diag}\{\alpha, \alpha, \varepsilon_z\}$ and $\overleftrightarrow{\mu} = \mathrm{diag}\{\varsigma, \varsigma, \mu_z\}$. For the sake of simplicity, we assume $\alpha = \varsigma = \mathrm{const}$ and

$$\varepsilon_z = 1 + f_1\omega_0^2/(\omega_0^2 - \omega^2), \quad \mu_z = 1 + f_2\omega^2/(\omega_0^2 - \omega^2), \quad (1)$$

where ω_0 indicates the resonance frequency and coefficients f_1 and f_2 are constants determined by the structure parameters which are adjustable. The presence of resonance along the z direction for both permittivity and permeability indicates that there exist two bulk plasmon modes, a longitudinal electric mode, and a longitudinal

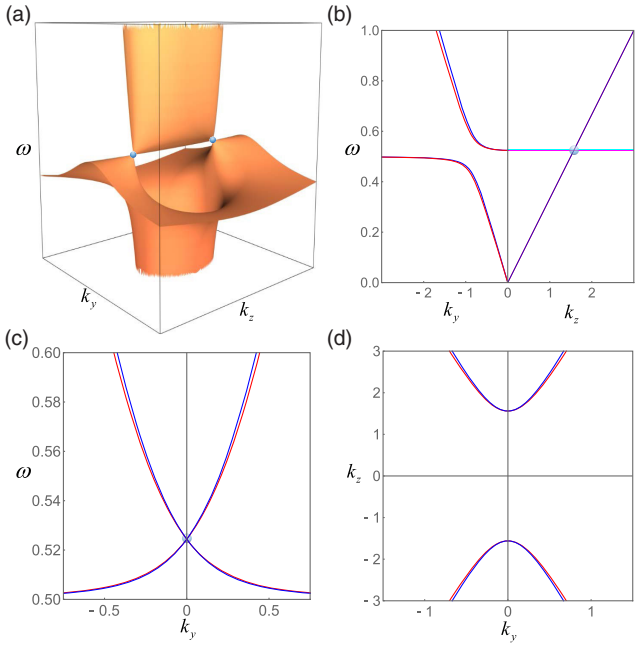

FIG. 1. Band structure of bulk states with $\alpha = \varsigma = 3$. (a) Effective bulk band structure on the k_y-k_z plane with the Dirac points marked by blue spheres. (b) The dispersion relation along the k_y and k_z direction, respectively, while (c) gives the dispersion along the k_y direction with k_z fixed at the Dirac point. In both (b) and (c), the Dirac points are marked with the blue points. (d) Equifrequency contour at a frequency below the Dirac points, which indicates the hyperbolic property of the material corresponds to the Dirac cone.

magnetic mode. From Eq. (1), it is straightforward to show that the degeneracy between the two longitudinal modes can be reached by setting $f_2 = 1 - 1/(1 + f_1)$.

The band structures for a specific set of parameters satisfying the above condition are shown in Fig. 1. Figure 1(a) shows the plot of band structures in the k_y-k_z plane, where two bands are nearly overlapping with each other. There are two fourfold degeneracy points symmetrically displaced on the k_z axis, as marked by the blue spheres. These two points are the Dirac points that form the central focus of our study. Figure 1(b) gives the dispersion relation of the material along the k_y and k_z directions. In the k_z direction, the two longitudinal modes and the two transverse modes are perfectly degenerate, respectively, across the whole frequency range. The band crossing between the two transverse modes and the two longitudinal modes is guaranteed by the orthogonality between them. Very recently, the crossing between a single longitudinal plasmon mode and one circular polarization mode in hyperbolic chiral metamaterials [23] and magnetized plasma [17] was found to show a topological nature, exhibiting exotic properties of Weyl quasiparticles.

Figure 1(c) shows the linear dispersions along the k_x or k_y direction across the Dirac point, where bands are also degenerate in a frequency range around the Dirac point. The linear dispersions along all directions reveal a massless Dirac collective excitation. In the momentum space, the equifrequency contour (EFC) at a frequency slightly below the Dirac points is shown in Fig. 1(d). One could see that the EFC possesses double hyperbolas ($\varepsilon_z < 0$, $\mu_z < 0$), which is characteristic of a double hyperbolic metamaterial (DHM).

In the proposed Dirac metamaterial, the 3D Dirac points are protected by electromagnetic duality $\overleftrightarrow{\varepsilon} = \eta\overleftrightarrow{\mu}$ ($\eta > 0$)—an internal symmetry of the electromagnetic fields [24]. In the metamaterials described above, $\eta = 1$. Under the following set of basis, LCP[$\vec{E} = (\hat{x} - i\hat{y})/\sqrt{2}, \vec{H} = i\vec{E}$], $L_1(\vec{E} = \hat{z}, \vec{H} = i\vec{E})$ and RCP[$\vec{E} = (\hat{x} + i\hat{y})/\sqrt{2}, \vec{H} = -i\vec{E}$], $L_2(\vec{E} = \hat{z}, \vec{H} = -i\vec{E})$, the Dirac Hamiltonian of the metamaterial takes a block-diagonal form consisting of two Weyl degeneracies [25]:

$$H_D(\vec{k}) = \begin{bmatrix} H_W(\vec{k}) & \\ & H_W^*(\vec{k}) \end{bmatrix}, \tag{2}$$

where the induced Weyl Hamiltonian, arising from the linear crossing between a longitudinal mode L_1 and a circularly polarized transverse mode right-circularly polarized (RCP) [17], is given by

$$H_W(\vec{k}) = \begin{bmatrix} d_z k_z & d_x k_x - i d_y k_y \\ d_x k_x + i d_y k_y & 0 \end{bmatrix}, \tag{3}$$

where d_i is the corresponding velocity determined by specific material parameters. Each Dirac point consists of two decoupled Weyl points with a chirality of ± 1, respectively, as schematically shown in Supplemental Material [25]. The chirality of each Weyl node is determined by the intrinsic spin $s = \pm 1$ of the transverse mode involved, because both longitudinal modes are spinless ($s = 0$).

An angle-resolved reflectance spectrum provides an intuitive way to show how a Dirac node can be decomposed into two decoupled complex-conjugation related Weyl points. As shown in Fig. 2(a), a plane wave with a specific polarization state is illuminated around the Dirac node (the blue points at the interface). Here we assume an ideal case that the overall system is under electromagnetic duality; the Dirac metamaterials $\overleftrightarrow{\varepsilon} = \overleftrightarrow{\mu} = \{k_D, k_D, 0\}$ with Dirac points are located at $x < 0$, while the $x > 0$ semispace is occupied by an isotropic medium with $\overleftrightarrow{\varepsilon} = \overleftrightarrow{\mu} > k_D I$. Figures 2(b) and 2(c) show the reflected polarization states and phases with RCP or LCP incidence, respectively. Obviously, circular polarizations are the eigenstates of the system due to the electromagnetic duality. In the momentum space, one anticlockwise loop around the Dirac point with RCP or LCP incidence acquires a $2\pi/-2\pi$ reflection phase leading to the generation of a vortex beam in reflection [25], which directly maps out the

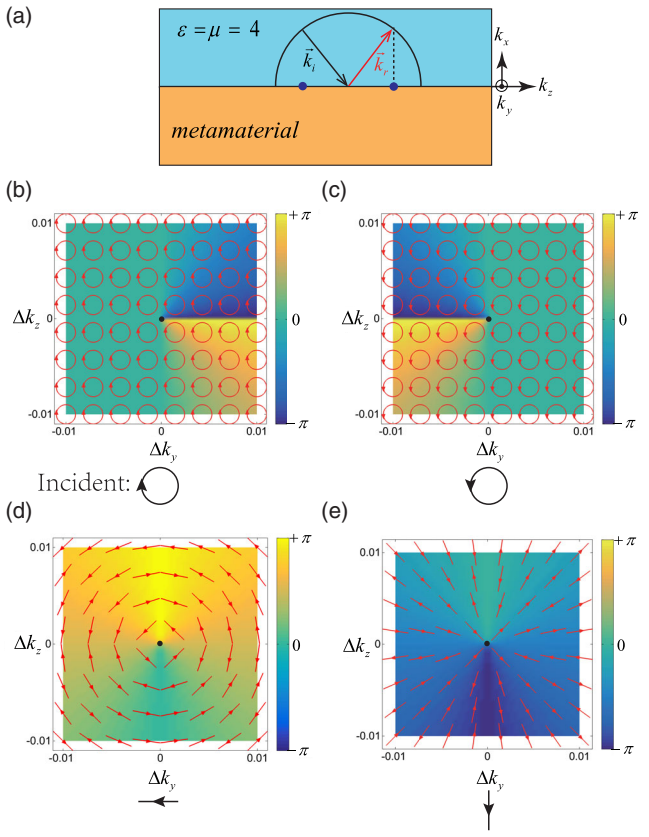

FIG. 2. Reflection spectrum around a Dirac point. (a) Configuration of the reflection calculation and Dirac points (two blue dots) in momentum space. One plane wave is incident $(\vec{k}_i)$ from the backgroud material $x > 0$ and totally reflected $(\vec{k}_r)$ back at the interface as indicated. (b) and (c) show the reflected E field with respect to right- or left-circular polarization incidence, respectively. (d) and (e) are similar to (b) and (c) with the incidences of two orthogonal linear polarizations. The incident polarization state is illustrated on the bottom of each panel.

chirality of each constituent Weyl point of the Dirac degeneracy. With linear polarization incidence, the reflection field is symmetric about the Δk_z axis as shown in Figs. 2(d) and 2(e). This can be understood as the topological charge of a Dirac node being 0. Interestingly, angular and radial vector beams are generated by a Gaussian beam incidence with TE and TM polarization states, respectively [Figs. 2(d) and 2(e)]. Therefore, the above study shows that 3D photonic Dirac points are topologically linked to the vector or vortex photonics. Dirac point degeneracy provides a novel method in generating vector and vortex beams.

As mentioned above, the Dirac point consists of two opposite Weyl points. A landmark of the Weyl topological phase is the existence of Fermi arcs connecting projections of pairs of Weyl points. Therefore, a topologically nontrivial Dirac point may exhibit double Fermi arcs, which have been observed in electronic systems [31]. Here we calculate the topological surface states between the Dirac metamaterials and air, where air naturally has electromagnetic duality symmetry $(\overleftrightarrow{\varepsilon}_{\text{air}} = \overleftrightarrow{\mu}_{\text{air}} = I)$. Furthermore, owing to the transverse nature of electromagnetic waves, the propagation of light in free space possesses Berry curvature in the momentum space given by $\vec{\Omega} = \sigma\vec{k}/|\vec{k}|^3$, where $\sigma = \pm 1$ represents the spin of RCP or LCP [32]. At the origin of momentum space, there exist singularities of Berry curvature, so-called "Dirac monopoles." For LCP the origin behaves like a sink of Berry flux, while for RCP it is the source. This nontriviality leads to the well-known spin-dependent Chern numbers 2σ. Thus, air provides topological nontriviality for the "Fermi arcs" connection [25].

As the duality symmetry between $\overleftrightarrow{\varepsilon}$ and $\overleftrightarrow{\mu}$ is preserved in both media, at the interface formed by these two media, there exist two pairs of spin-polarized surface states, as shown in Fig. 3(a). Each pair of surface states consists of spin-up ($\sigma = +1$, indicated with a magenta surface) and spin-down ($\sigma = -1$, indicated with a cyan surface) surface states [25]. Figure 3(b) shows the EFC of the Fermi-arc-like surface states at Dirac points. From each Dirac point, there are two Fermi arcs connecting to the air light circle. In Fig. 3(c), EFCs at a frequency below Dirac points are presented. Interestingly, by setting $\varepsilon_z = \mu_z = \beta$ with $(\alpha > 1, \beta \leq 0)$, these Fermi arcs geometrically appear as straight line segments tangentially connecting air-circle and DHM-hyperbolas with a linear dispersion relation in k space,

$$k_z = \pm\frac{\sqrt{\alpha^2 - 1}}{\sqrt{1 - \alpha\beta}}k_y \pm \frac{\sqrt{\alpha^2 - \alpha\beta}}{\sqrt{1 - \alpha\beta}}, \tag{4}$$

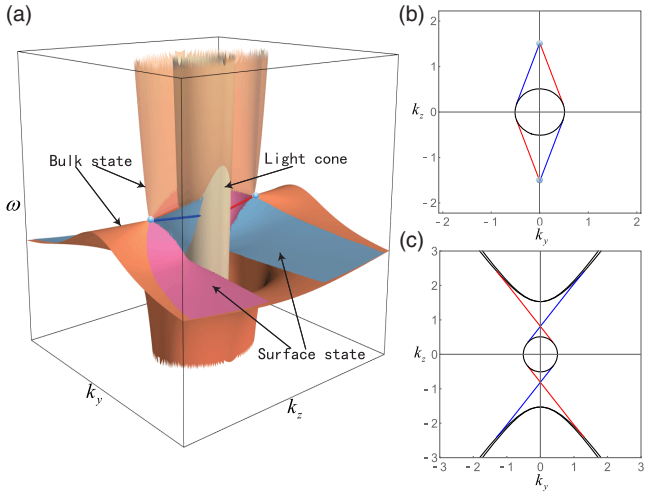

FIG. 3. Bulk and surface states of the effective medium. (a) 3D band structures of bulk and surface states of the effective medium. The spin-up (spin-down) surface state between two Dirac points and the vacuum is indicated by the magenta (cyan) surface. The blue and red lines highlight the photonic Fermi arcs at Dirac points. Equifrequency contours at two different frequencies could be seen in (b) and (c) corresponding to the frequency at the Dirac point and below it, respectively. The red and blue lines in (b) and (c) represent the spin-up and spin-down topological surface states, while the black lines represent the effective material and vacuum bulk states.

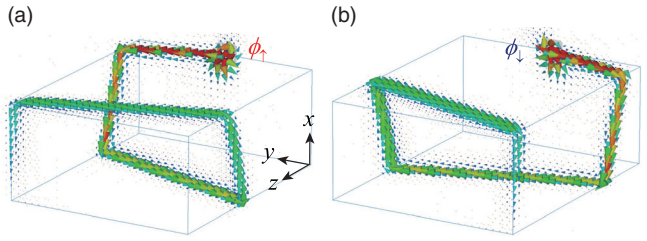

FIG. 4. Surface states indicated by power flow simulated in 3D by CST time domain. The (a) spin-up and (b) spin-down surface states propagate helically along the z direction clockwise and anticlockwise, respectively, on the surface of cuboid effective material which is capsulated by a vacuum.

which leads to the near-diffractionless propagation of the surface state. The length of the surface dispersion segments is found to be strictly related to the decay constant in both air and a DHM [25].

In order to demonstrate the topological protection and spin-momentum locking of the surface states, a full wave 3D simulation is performed using CST MICROWAVE STUDIO with parameters of $\alpha = 3$, $\beta = 0$ (at the Dirac point frequency). The configuration is built by a cuboid-shaped Dirac metamaterial surrounded by air. A small port is positioned at the interface as the radiation source. Figures 4(a) and 4(b) show the backscattering immune transportation of spin-dependent surface waves helically bending around z-invariant sharp corners, indicating the one-way surface state is right- or left-handed polarization [25]. These demonstrations confirm the robustness of spin Fermi arcs in the photonic Dirac metamaterials.

Having outlined the realization of Dirac points in metamaterials based on their effective parameters, we now demonstrate the experimental feasibility of our scheme by designing a realistic metamaterial structure. To simultaneously realize the required permittivity and permeability dispersion along the z direction, we apply metallic helixes as shown in Fig. 5(a), where two mirrored helixes along the z direction (clockwise- and anticlockwise-rotated helix pair) to introduce both electric and magnetic resonances along the z direction while eliminating the chiral response. In the x-y plane, we apply C_4 rotation symmetry to achieve an in-plane isotropic electromagnetic response. Thus, each unit cell consists of eight helixes in total. By tuning the geometric parameters of the structure, such as radius R, height h, period P along the x or y direction, and p_z along the z direction, the dispersion of ε_z and μ_z can be adjusted, leading to the degeneracy of the two longitudinal modes. In the microwave regime, the designed Dirac metamaterial can be readily fabricated [23,33]. Figures 5(b) and 5(c) present the dispersion curves of the bulk states of the proposed metamaterial along the z and y directions, respectively. The presence of a fourfold crossing between two degenerate longitudinal modes (Fig. S5, L1 and L2) and two degenerate transverse modes (Fig. S5, T1 and T2) is observed [25]. Furthermore, the presence of Fermi-arc-like surface states is numerically confirmed as shown in Fig. 5(d),

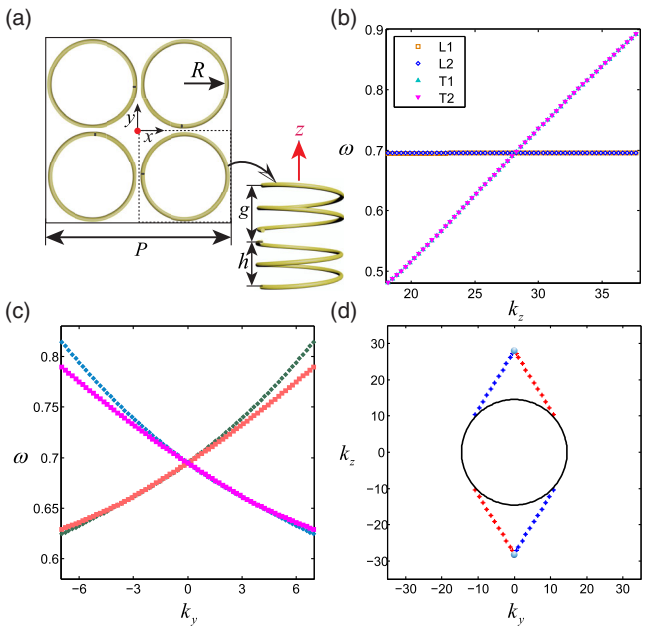

FIG. 5. Dirac points with a realistic metamaterial structure. (a) The metamaterial structure with a top view of one unit cell composed with C_4 symmetry distributed helix pairs and the front view of a pair of mirrored helixes with opposite rotation directions with parameters $R = 20$ mm, $p_x = p_y = P = 90$ mm, $p_z = 50$ mm, $g = 25$ mm, and $h = 20$ mm. (b) and (c) are the simulated band structure of the metamaterial along the k_z and k_y direction, respectively. (d) Surface state dispersion at the Dirac point frequency (0.695 GHz). Frequency and wavevector are in units of GHz and degree, respectively.

where a supercell consisting of 20 unit cells surrounded by air is used in the surface state calculation. The localization of the surface states is shown in Fig. S6 [25].

The Dirac point here lies right at the critical transition between type I and type II. This is due to the flat dispersion relation of the bulk plasmon modes. For a type-I Dirac point, the EFC reduces to a single point in the momentum space, while for a type-II Dirac point, the EFC consists of two touching cones. For the transitional Dirac point described here, the EFC is a straight line which corresponds to the degenerate electric and magnetic bulk plasmon modes. On the other hand, it is possible to introduce nonlocality into the system such that the bulk plasmon dispersion is not flat but exhibits either positive or negative dispersion [20]. That would lead to the construction of either type-I or type-II Dirac points. Note that type-II Dirac points in a photonic crystal were proposed in Ref. [21], where spatial degrees of freedom play a key role in constructing the state space around Dirac points. In contrast, the Dirac points discovered here exploit the internal degrees of freedom of the electromagnetic wave that arise from the orthogonality between different polarization states. Therefore, our scheme represents an intrinsic way towards realizing photonic Dirac points.

The exploration of topological photonics protected by electromagnetic duality symmetry has introduced a number

of intriguing optical phenomena [9,12,34]. However, the experimental observation still remains challenging, particularly in 3D up to now. It is expected that a well-developed metamaterials theory and finely designed high-permittivity metacrystals [12] can provide an electromagnetic duality platform to discovery more new photonic topological phases.

In conclusion, by considering electromagnetic duality symmetry, we theoretically proposed the realization of photonic Dirac degeneracy and spin-dependent Fermi-arc-like surface states. This theoretical model is of great importance in understanding fundamental topological photonics, such as exhibiting transition from a Z_2 topological insulator to Weyl degeneracies [4]. Furthermore, the fundamental link between photonic Dirac points and vector or vortex optics has been established through optical reflection with in-plane momentum matching the Dirac points. The concept of Dirac point may also be extended from the momentum space to a synthetic space, where synthetic Weyl points were recently discovered [35].

The work is partially supported by ERC Consolidator Grant (TOPOLOGICAL), the Royal Society and the Wolfson Foundation, Leverhulme Trust (RPG-2012-674), and Horizon 2020 Action, Project No. 734578 (D-SPA). Q. G. acknowledges the financial support by National Science Foundation of China (Grant No. 11604216) and China Postdoctoral Science Foundation (Grant No. 2016M600667). B. Y. acknowledges China Scholarship Council (201306110041). J. C. acknowledges support from the National Natural Science Foundation of China (Grant No. 11574162). Y. X. acknowledges support from the National Natural Science Foundation of China (Grants No. 61490713 and No. 61505111).

Q. G. and B. Y. contributed equally to this work.

*xiangyuanjiang@126.com
†s.zhang@bham.ac.uk

[1] X.-L. Qi and S.-C. Zhang, Rev. Mod. Phys. **83**, 1057 (2011).
[2] M. Z. Hasan and C. L. Kane, Rev. Mod. Phys. **82**, 3045 (2010).
[3] C.-K. Chiu, J. C. Y. Teo, A. P. Schnyder, and S. Ryu, Rev. Mod. Phys. **88**, 035005 (2016).
[4] N. P. Armitage, E. J. Mele, and A. Vishwanath, arXiv: 1705.01111 [Rev. Mod. Phys. (to be published)].
[5] K. v. Klitzing, G. Dorda, and M. Pepper, Phys. Rev. Lett. **45**, 494 (1980).
[6] F. D. M. Haldane and S. Raghu, Phys. Rev. Lett. **100**, 013904 (2008).
[7] Z. Wang, Y. Chong, J. D. Joannopoulos, and M. Soljacic, Nature (London) **461**, 772 (2009).
[8] M. C. Rechtsman, J. M. Zeuner, Y. Plotnik, Y. Lumer, D. Podolsky, F. Dreisow, S. Nolte, M. Segev, and A. Szameit, Nature (London) **496**, 196 (2013).
[9] A. B. Khanikaev, S. Hossein Mousavi, W.-K. Tse, M. Kargarian, A. H. MacDonald, and G. Shvets, Nat. Mater. **12**, 233 (2013).
[10] W.-J. Chen, S.-J. Jiang, X.-D. Chen, B. Zhu, L. Zhou, J.-W. Dong, and C. T. Chan, Nat. Commun. **5**, 5782 (2014).
[11] L. Lu, C. Fang, L. Fu, S. G. Johnson, J. D. Joannopoulos, and M. Soljacic, Nat. Phys. **12**, 337 (2016).
[12] A. Slobozhanyuk, S. H. Mousavi, X. Ni, D. Smirnova, Y. S. Kivshar, and A. B. Khanikaev, Nat. Photonics **11**, 130 (2017).
[13] L. Lu, L. Fu, J. D. Joannopoulos, and M. Soljacic, Nat. Photonics **7**, 294 (2013).
[14] L. Lu, Z. Wang, D. Ye, L. Ran, L. Fu, J. D. Joannopoulos, and M. Soljačić, Science **349**, 622 (2015).
[15] W. Gao, M. Lawrence, B. Yang, F. Liu, F. Fang, B. Béri, J. Li, and S. Zhang, Phys. Rev. Lett. **114**, 037402 (2015).
[16] E. E. Narimanov, Faraday Discuss. **178**, 45 (2015).
[17] W. Gao, B. Yang, M. Lawrence, F. Fang, B. Béri, and S. Zhang, Nat. Commun. **7**, 12435 (2016).
[18] H. X. Wang, L. Xu, H. Y. Chen, and J.-H. Jiang, Phys. Rev. B **93**, 235155 (2016).
[19] W.-J. Chen, M. Xiao, and C. T. Chan, Nat. Commun. **7**, 13038 (2016).
[20] M. Xiao, Q. Lin, and S. Fan, Phys. Rev. Lett. **117**, 057401 (2016).
[21] H.-X. Wang, Y. Chen, Z. H. Hang, H.-Y. Kee, and J.-H. Jiang, npj Quantum Mater. **2**, 54 (2017).
[22] J. Noh, S. Huang, D. Leykam, Y. D. Chong, K. P. Chen, and M. C. Rechtsman, Nat. Phys. **13**, 611 (2017).
[23] B. Yang, Q. Guo, B. Tremain, L. E. Barr, W. Gao, H. Liu, B. Béri, Y. Xiang, D. Fan, A. P. Hibbins, and S. Zhang, Nat. Commun. **8**, 97 (2017).
[24] I. Fernandez-Corbaton, X. Zambrana-Puyalto, N. Tischler, X. Vidal, M. L. Juan, and G. Molina-Terriza, Phys. Rev. Lett. **111**, 060401 (2013).
[25] See Supplemental Material at http://link.aps.org/supplemental/10.1103/PhysRevLett.119.213901 for effective Hamiltonian analysis, nontrivial topology of air-DHM systems, analytical solution to surface states and photonic Dirac metamaterials design, which includes Refs. [26–30].
[26] A. Raman and S. Fan, Phys. Rev. Lett. **104**, 087401 (2010).
[27] M. I. Dyakonov, Sov. Phys. JETP **67**, 714 (1988).
[28] M. Wada, S. Murakami, F. Freimuth, and G. Bihlmayer, Phys. Rev. B **83**, 121310 (2011).
[29] D. R. Smith, S. Schultz, P. Markoš, and C. M. Soukoulis, Phys. Rev. B **65**, 195104 (2002).
[30] F. Tianhua, L. Fu, T. Wing Yim, and L. Jensen, Europhys. Lett. **102**, 18003 (2013).
[31] S.-Y. Xu, C. Liu, S. K. Kushwaha, R. Sankar, J. W. Krizan, I. Belopolski, M. Neupane, G. Bian, N. Alidoust, T.-R. Chang, H.-T. Jeng, C.-Y. Huang, W.-F. Tsai, H. Lin, P. P. Shibayev, F.-C. Chou, R. J. Cava, and M. Z. Hasan, Science **347**, 294 (2015).
[32] K. Y. Bliokh, D. Smirnova, and F. Nori, Science **348**, 1448 (2015).
[33] W. Bingnan, Z. Jiangfeng, K. Thomas, K. Maria, and M. S. Costas, J. Opt. A **11**, 114003 (2009).
[34] J.-W. Dong, X.-D. Chen, H. Zhu, Y. Wang, and X. Zhang, Nat. Mater. **16**, 298 (2017).
[35] Q. Wang, M. Xiao, H. Liu, S. Zhu, and C. T. Chan, Phys. Rev. X **7**, 031032 (2017).